GL03933

Relaxation of Geothermal Reservoir

Stresses Induced by Heat Production

H. Murphy, Editor

R. Aamodt	H. Keppler*
H. Fisher	C. Pearson
T. Grant	R. Potter
C. Grigsby	G. Suhr**
R. Hendron	G. Zyvoloski

*Alien Guest Scientist. Federal Institute for Geosciences and National Resources
(B.G.R.), Hannover, FEDERAL REPUBLIC OF GERMANY.
**Alien Guest Scientist. Prakla-Seismos, Hannover, FEDERAL REPUBLIC OF GERMANY.

RELAXATION OF GEOTHERMAL RESERVOIR STRESSES INDUCED BY HEAT PRODUCTION

by

H. Murphy (Ed.), R. Aamodt, H. Fisher, T. Grant, C. Grigsby, R. Hendron,
H. Keppler, C. Pearson, R. Potter, G. Suhr, and G. Zyvoloski

ABSTRACT

Fifteen million kWh of thermal energy were
produced during 281 days of operation of the hot
dry rock (HDR) geothermal reservoir at Fenton Hill,
New Mexico. Following this heat production the
thermal stresses and strains so induced were par-
tially released by a short, 7-h pressurization of
the reservoir above the local tectonic confining
stress. Following the partial stress release, it
was found that the resistance to water flow through
the reservoir was decreased by 37%, and that the
reservoir volume, as measured by tracer studies,
increased by 43%. Microseismic events recorded
with geophones in two deep wells at positions
within a few hundred meters of the reservoir were
concentrated in those regions of the reservoir most
affected by thermal depletion. These events define
a reservoir region and size in qualitative agree-
ment with estimates based upon heat production
modeling.

I. INTRODUCTION

On December 9 and 10, 1980, after 281 days of sustained heat extraction
that took place during Run Segment 5, the stress unlocking experiment (SUE)
was conducted. Run Segment 5 was the latest in a series of tests of the hot
dry rock (HDR) geothermal reservoir at Fenton Hill, in the Jemez Mountains of
northern New Mexico. The results of Run Segment 5, as well as a general de-
scription and historical background of the HDR geothermal project are reported
in Ref. 1. The stress unlocking experiment had four purposes:

(1) Produce acoustic signals, that is, microseismicity from the produced geothermal reservoir by releasing the accumulated thermal strains and stresses produced by 281 days of sustained heat extraction and rock cooling. At the time of the SUE experiment about 15 000 000 kWh of thermal energy had been extracted from the reservoir. The relaxation of thermal stresses was accomplished by pumping water in the reservoir injection well, EE-1, at high pressures, about 15 MPa (2200 psi). Because the reservoir production well, GT-2B, was shut-in, or also pressurized, nearly the entire reservoir was pressurized to high levels, and it was hoped that the normal forces that held the fracture faces together in frictional contact would be reduced, resulting in shear slippage and microseismicity. Monitoring of microseismic signals was performed with two downhole geophone packages, one stationed in GT-2B (the usual reservoir production well) and the other in EE-2 (a recently drilled well) that served as an observation well for this experiment.

(2) Reduce the fracture flow impedance as a consequence of the shear-slippage of fracture faces.

(3) Provide the first cycle of a Huff-Puff mode of reservoir heat extraction. The usual mode of heat extraction is a steady-flow-circulation mode in which flow is injected at a constant rate in the injection well and withdrawn steadily at the production well. The heat extraction in this mode is limited by the fluid streamline patterns and may not reflect the heat extraction potentially available from the total fracture area. Huff-Puff operation is cyclical. Fluid is first injected without withdrawal, thus inflating the fractures, and after a thermal "soak" time the fluid is then withdrawn.

(4) Investigate the possibility of studying changes in reservoir spectral pressure responses due to increased reservoir size or reduced flow impedance.

Pumping at the flow rates and pressure levels intended for SUE was beyond the Los Alamos circulating pumps. Consequently, pumping services were rented from the Halliburton Company for the occasion. One low-pressure pump truck, normally used for blending purposes, and three high-pressure pump trucks, usually used for fracturing operations, were provided. The cost of renting this equipment, and the operators required to man the equipment, was $13 300. Only one high-pressure truck was actually required, the other two remained on standby. The pump trucks were arranged so that the blender took water from the GT-2B pond and the so-called "black" storage tank, which holds 150 m^3

(40 000 gal). The blender was connected to the black tank, and water was transferred from the pond to this tank by the Los Alamos "supercharger" pump. This water was then pumped to the high-pressure pump, which raised the pressure and injected the water into either EE-1 or GT-2B, depending upon the phase of the experiment. The high-pressure pump was plumbed into the loop piping near the EE-1 wellhead, just upstream of flow control valve 1. Injection flow rates were measured with a Halliburton-supplied 4-in. turbine flow meter.

SUE consisted of three main phases: (1) injection into EE-1, (2) injection into GT-2B, and (3) venting from GT-2B. A fourth phase, the impedance measurement immediately following SUE, was technically not a part of SUE, but the results of this measurement are included in this report for completeness. Phase (1), EE-1 pumping with the Halliburton trucks, started at about 15:00 on December 9. This initial Halliburton pumping was conducted at 0.0074 m^3/s (118 gpm), corresponding to the usual circulating rate that prevailed in Run Segment 5 just prior to SUE; the purpose was simply to switch from Laboratory to Halliburton pumping as smoothly as possible and reestablish typical Run Segment 5 conditions prior to the first high-flow-rate step of Phase 1. This switch in pumping systems and the subsequent pumping steps are shown in Fig. 1.

The first high-rate pumping step began at 16:00 at 0.013 m^3/s (210 gpm), and as shown in Fig. 1, was succeeded by two more steps at 0.027 and 0.047 m^3/s (420 and 750 gpm). In the sustained EE-1 pressurization that followed the 0.047-m^3/s step, the flow rate was adjusted slightly, to a final value of 0.042 m^3/s (660 gpm), roughly in balance with the less-than-expected pumping capacity of the supercharger pump that transported water from the GT-2B pond to the black tank. Following the injection volume of 1000 m^3 (270 000 gal), the planned amount, EE-1 was shut in at 23:00 and Phase (2), injection into GT-2B at approximately 0.026 m^3/s (420 gpm), was started. The GT-2B flow was injected through the buried 73-mm (2-7/8-in.) pipe from the EE-1 area to the GT-2 wellhead. An increase of pumping rate to 0.030 m^3/s was accomplished about halfway through the planned 38-m^3 (10 000-gal) GT-2B injection. Just as the end of the total GT-2B injection was approached, piping vibrations were noted at GT-2B, and Halliburton flow jumped to 0.069 m^3/s (1090 gpm). No such gyrations were recorded in the CDA. Pumps were shut down immediately at 23:23. Maximum GT-2B pressure during the injection was 13 MPa (1890 psi). At 23:24, following the injection of the 38 m^3, GT-2 was shut in.
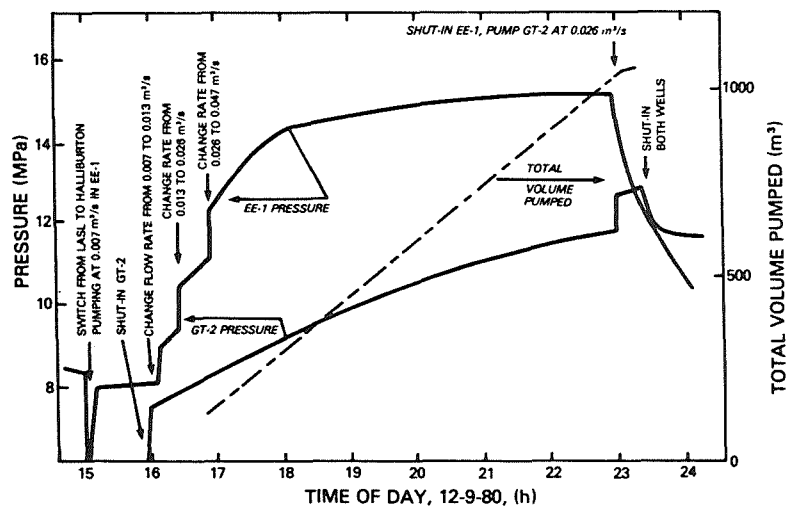
3

Fig. 1.
Major system parameters during SUE.

The GT-2B injection volume was limited to 38 m^3 to avoid significant thermal perturbation to the normally hot production well, which could have resulted in damage to the casing cement. The EE-1 injection was limited to 1000 m^3 because the combined injections, about 1040 m^3, were equal to the total storage capacity in the GT-2B pond and the black tank. Following the GT-2B shut-in, the pressure in both wells decreased slowly.

Phase (3), the vent from both GT-2B and the continuing leak from the EE-1 annulus, was started on 12-10-80 at 00:47. The flow rate from GT-2B varied from 0.012 to 0.014 m^3/s (190 to 220 gpm) as the control valve FCV-2 was periodically opened. Seismic monitoring was terminated at 00:52 and the geophone tool was removed from EE-2. The GT-2 tool was raised at 03:30 to 55 m (180 ft) and parked with the arm extended. The loop was readied for easy change from vent to circulating mode at the same time. Venting was first run through the temporary surface transfer line from the EE-1 area to the GT-2 pond. Initial venting seemed to indicate a very quick pressure drop and return to loop operations and impedance testing. By the time loop preparations were made the pressures were decreasing slowly and venting continued into EE-1 pond and then to GT-2 pond. At 04:16 the flow rate dropped below 0.013 m^3/s and the GT-2B control valve was opened all the way. By 06:00 the EE-1 pressure was 8.3 MPa (1200 psi); GT-2B was 1.1 MPa (165 psi) and venting at 0.012 m^3/s (180 gpm). The annulus flow rate was 0.002 m^3/s (30 gpm). The wellhead

4

pressures were thus approximately those prevailing prior to the SUE injections, so closed-loop operation was reestablished at 06:20, December 10, in order to measure the post-SUE impedance. The system operated while venting through the EE-1 annulus and FCV-3 with no make-up until 07:45, December 11. Loop-operating data then provided information for an impedance calculation. On Thursday, December 11, the system was shut in from 13:00 to 14:50 to change pump seals for the final NH_4 Br^{82} tracer experiment of Segment 5. The tracer was injected in EE-1 at 12:50, December 12 and monitored in EE-1 until 23:14, December 14. A spinner/temperature survey in GT-2B was performed on December 15. The NH_4 Br concentration in the fluid produced from GT-2B was monitored until loop shut-down, which occurred on December 16, 1980 at 09:00.

During SUE the annulus leak flow rate at EE-1 increased from 0.0015 m^3/s (24 gpm) at the beginning of the experiment to a maximum of 0.0037 m^3/s (59 gpm); the maximum occurred about 18 min after cessation of the injection into GT-2B.

Analyses of the EE-1 and GT-2B pressure rises that accompanied the injection rate steps of phases (1) and (2) are described in the next main section. Also found in this section are analyses of the vent, phase (3), and implications for the Huff-Puff mode of heat extraction with the reservoir. Following these pressure-transient analyses is a preliminary report on the microseismic observations during the pressurization phases (1) and (2) and another section dealing with the pressure oscillations. This is then followed by our analysis of impedance and fracture volume changes caused by SUE. The final section lists our conclusions.

II. PRESSURE-TRANSIENT ANALYSES

The pressure data used in this section are all raw data and are not corrected for buoyancy. In Sec. V, in which buoyancy corrections are important for impedance determinations, such corrections are incorporated.

A. Phase (1), EE-1 Injection

The EE-1 flow rates and pressures for each of the high-flow-rate steps are plotted in detail for each flow step in Figs. 2, 3, and 4. In Fig. 2 the flow data are somewhat sparse because of a transducer malfunction and in fact some of the data were transmitted by the Halliburton operator. The pressure response to the flow steps indicates a fairly complex system. However, a few tentative findings can be reported.
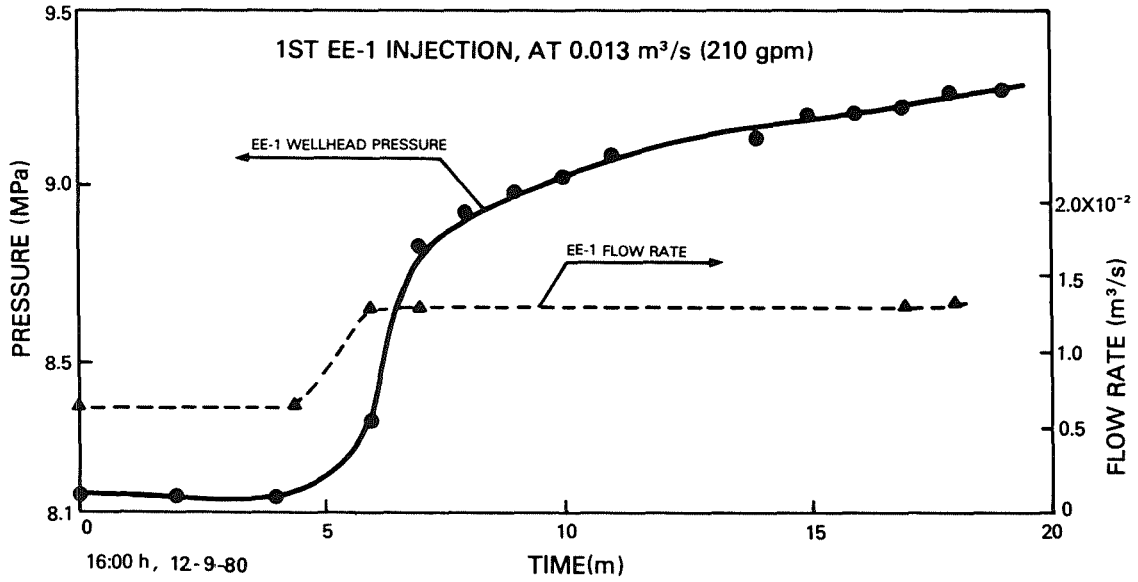
Fig. 2.
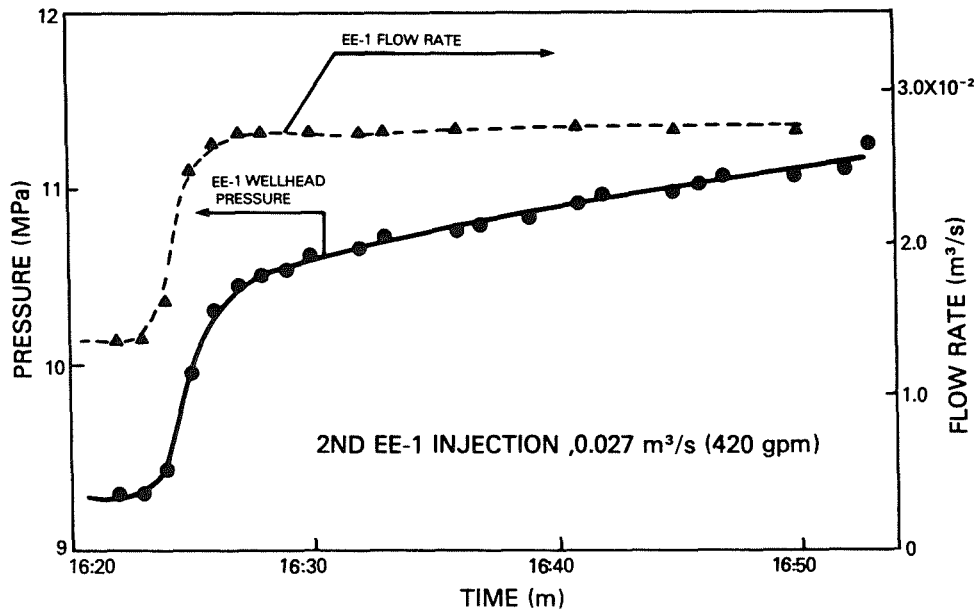EE-1 pressure and flow rate during first EE-1 injection.

Fig. 3.
EE-1 pressure and flow rate during second EE-1 injection.

6

Each pressure response has a rapid initial rise that corresponds to the increase of flow rate. This can be attributed to an input impedance located near the EE-1 wellbore. The resulting input-impedance values are plotted in Fig. 5 as a function of the starting pressure at the beginning of each flow-rate step. These values also probably contain some flow dependence. In Figs. 2, 3, and 4 each rapid rise of pressure is followed by a period in which the pressure increase is approximately proportional to the square root of time. This defines a receptivity (Ref. 1) that is also plotted in Fig. 5. There is no particular correlation with pressure. However, this interpretation of the data is not unique and the diffusion receptivity is also a function of flow rate.

B.   Phase (2), GT-2B Injection

Starting at 23:00, December 9, EE-1 was shut in and we began injection into GT-2B at the rate of 0.026 m^3/s (420 gpm) for approximately 25 minutes. The resulting pressure response is plotted in Fig. 6. The entrance impedance at GT-2B was reduced to about 20 MPa s/m^3 (0.2 psi/gpm) by the high resulting GT-2B pressure. This impedance value pertains only to operation with GT-2B at the pressures shown, about 12 MPa (1700 psi). Such a pressure would represent an extreme case of "high-back-pressure" (HBP) operation. Operation at more normal, low back pressure (LBP) of about 1.4 MPa (200 psi) would result in additional fracture closure. As will be seen in Sec. V, this closure results in a LBP impedance of 0.6 GPa s/m^3 (5.5 psi/gpm). Although high in comparison to HBP operation, this LBP exit impedance is still about one-half what it was before SUE.

C.   Phase (3), The GT-2B Vent

Figures 7 and 8 show the details of the pressure and flow histories during the shut-in of both wells prior to the GT-2B vent and during the vent itself. Actually shown in Fig. 8 is the EE-1 annulus leak rate, which, as mentioned in the introduction, reached a maximum of 0.0037 m^3/s (59 gpm) during the shut-in. During the vent a total of 345 m^3 (91 000 gal) of water was recovered. Of this, 270 m^3 was recovered at GT-2B and 75 m^3 was recovered from the EE-1 annulus.

After the beginning of the vent at 00:47 on December 10, the GT-2B pressure decreased nearly linearly with time as the GT-2B control valve was opened to maintain a flow of 0.012 to 0.014 m^3/s. After the GT-2B pressure reached 1.4 MPa and was maintained at this value, the GT-2B flow decreased slowly to
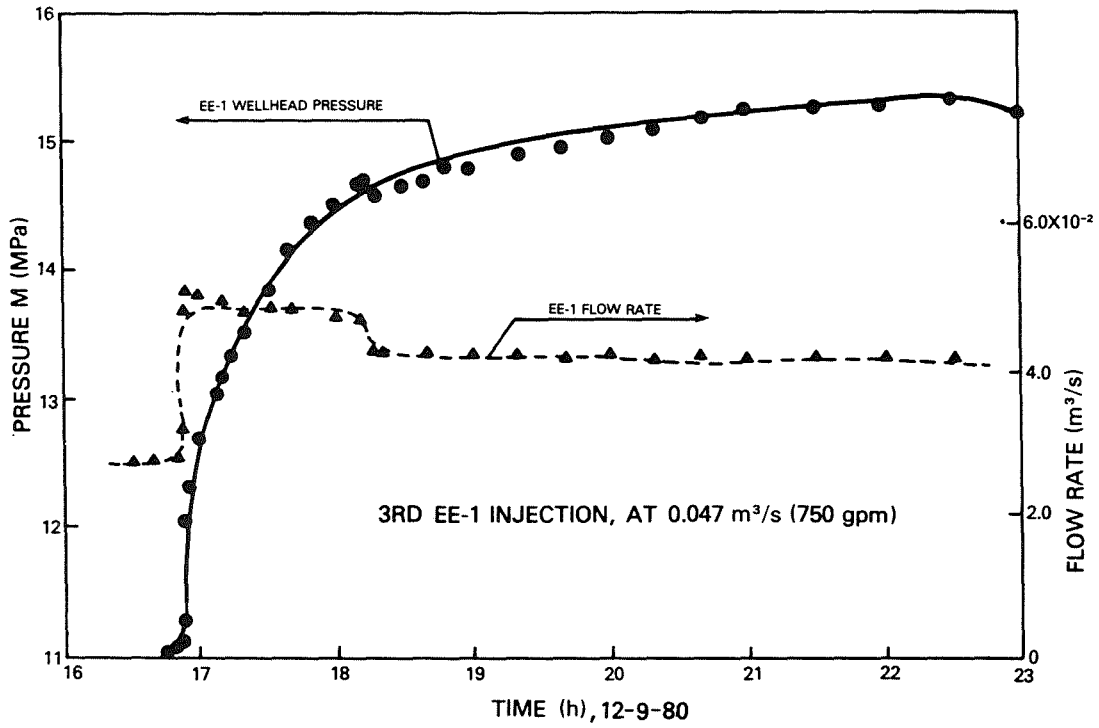
Fig. 4.
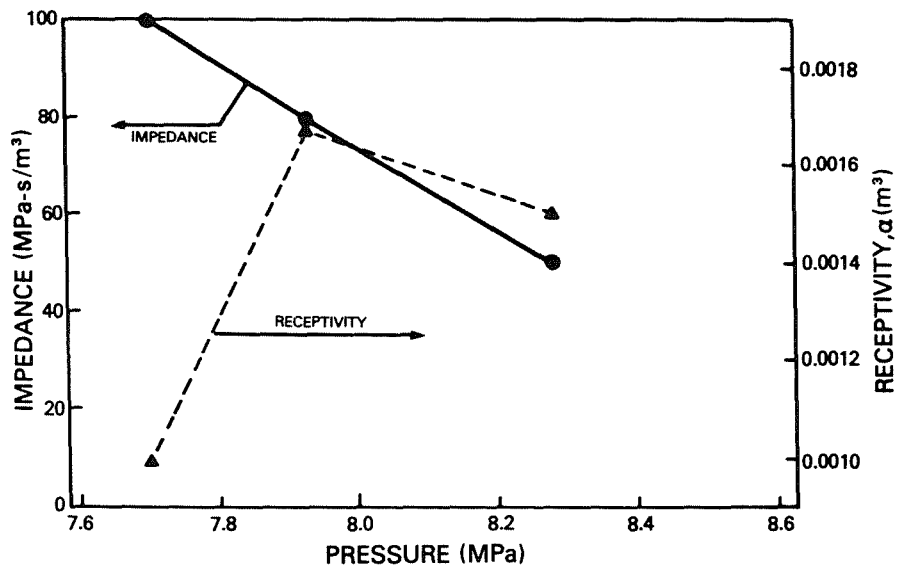EE-1 pressure and flow rate during third EE-1 injection.

Fig. 5.
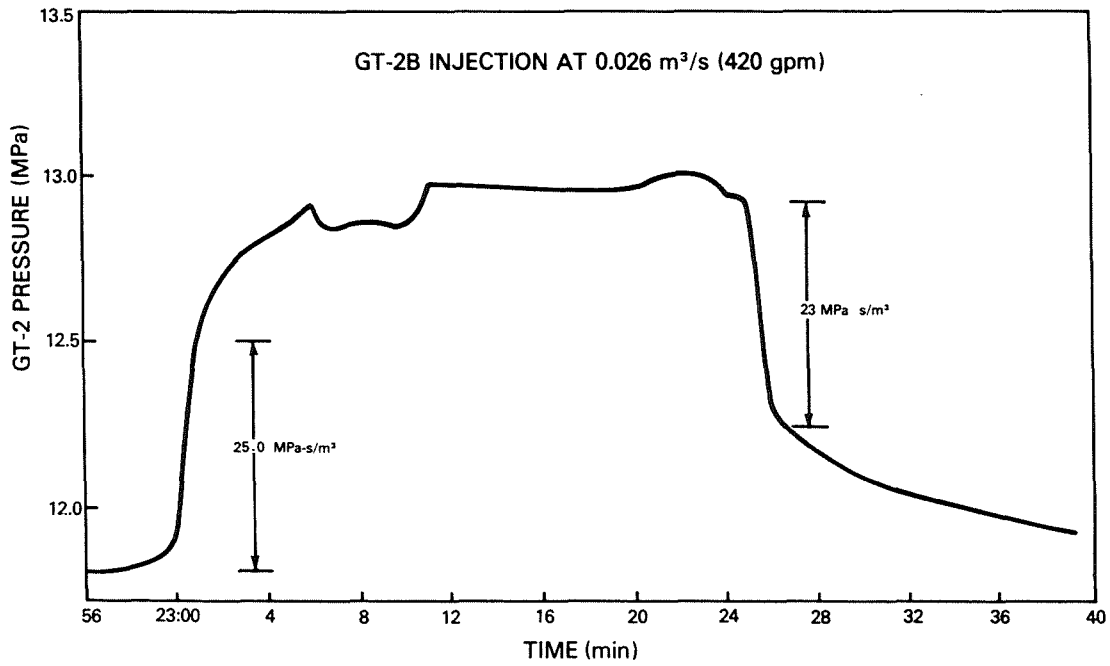EE-1 input impedance and receptivity.
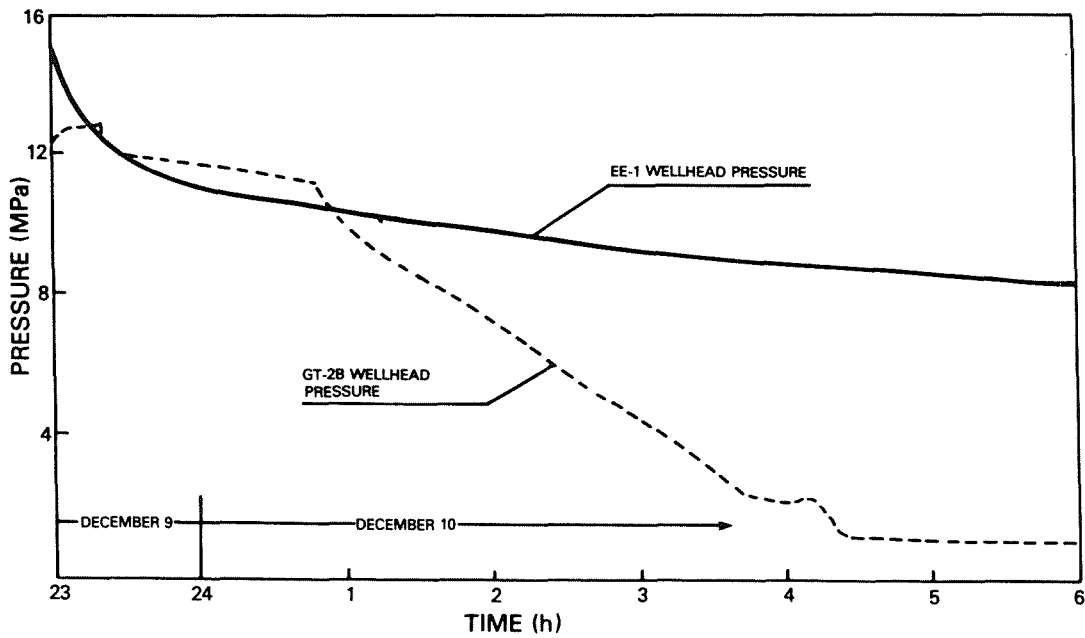
Fig. 6.
GT-2B pressure during GT-2B injection.
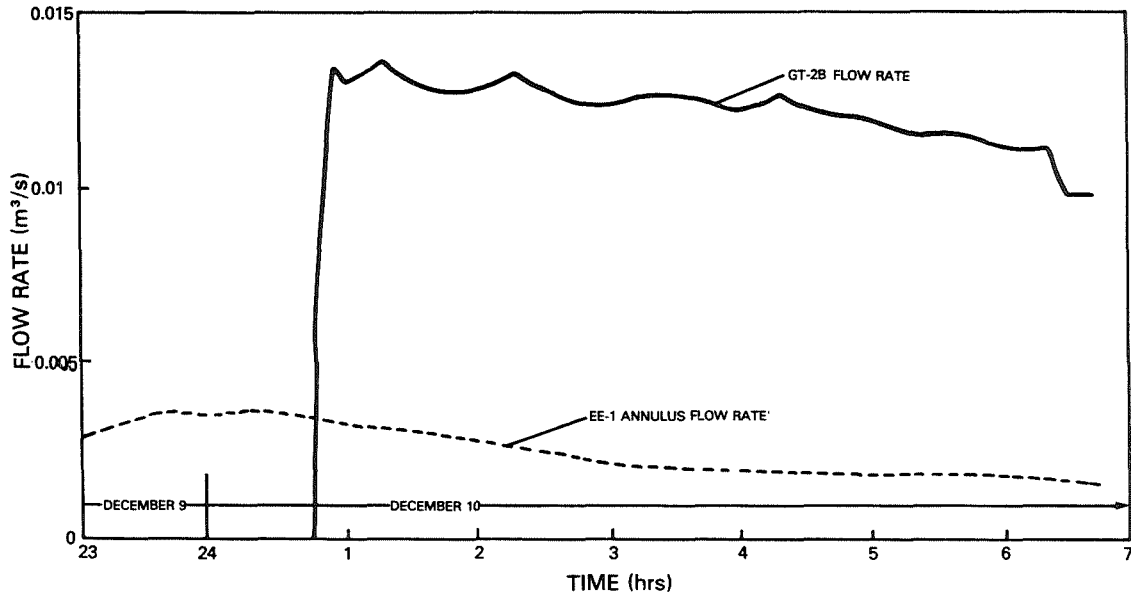

Fig. 7.
Wellhead pressures during shut-in and vent.

Fig. 8.
Flow rates during shut-in and vent.

0.011 m^3/s. This gradual decrease of the GT-2B pressure, P_2, and almost constant GT-2B flow, Q_2, can be explained in terms of a simple pressure dependence of exit impedance $I_2(P_2)$. The argument, P_2, of the exit impedance expresses concretely the above concept that I_2 is a function of P_2. The exit impedance at LBP ($P_2 \sim 0$) is designated as $I_2(0)$. If we <u>assume</u> that the slow decay of both P(EE-1) and P_2 during the shut-in means that the reservoir pressure (P_R) does not decrease rapidly during the vent, then

$$I_2(P) = \frac{P_R - P_2}{Q_2} \quad .$$

(1)

Because Q_2 was observed to remain roughly constant and P_R is assumed constant, Eq. (1) can be rewritten in the form

$$I_2(P) = I_2(0) \left(1 - \frac{P_2}{P_r}\right) \quad .$$

(2)

Using the data from the vent in Eq. (2), it can be shown that

$$I_2(0) = 0.84 \text{ GPa s/m}^3 \text{ (7.5 psi/gpm) and } P_r = 10 \text{ MPa} \quad .$$

10

This value of LBP exit impedance, $I_2(0) = 0.84$ GPa s/m^3, compares favorably with the value 0.6 GPa s/m^3 obtained in the usual loop operating manner during the impedance measurement following SUE (see Sec. V). The pressure dependency of $I_2(P)$ was determined from the vent data and Eq. (1) and is compared in Fig. 9 with other measurements made immediately before. This linear dependence of impedance on pressure has been observed previously (Refs. 1 and 2) and is discussed in detail in Ref. 1.

D.   Huff-Puff Implications

The inflation and vent of the system was also used to evaluate those characteristics of the system that would affect two-port huff-puff operation. Of particular interest are the water loss per cycle, the vent volume, and the
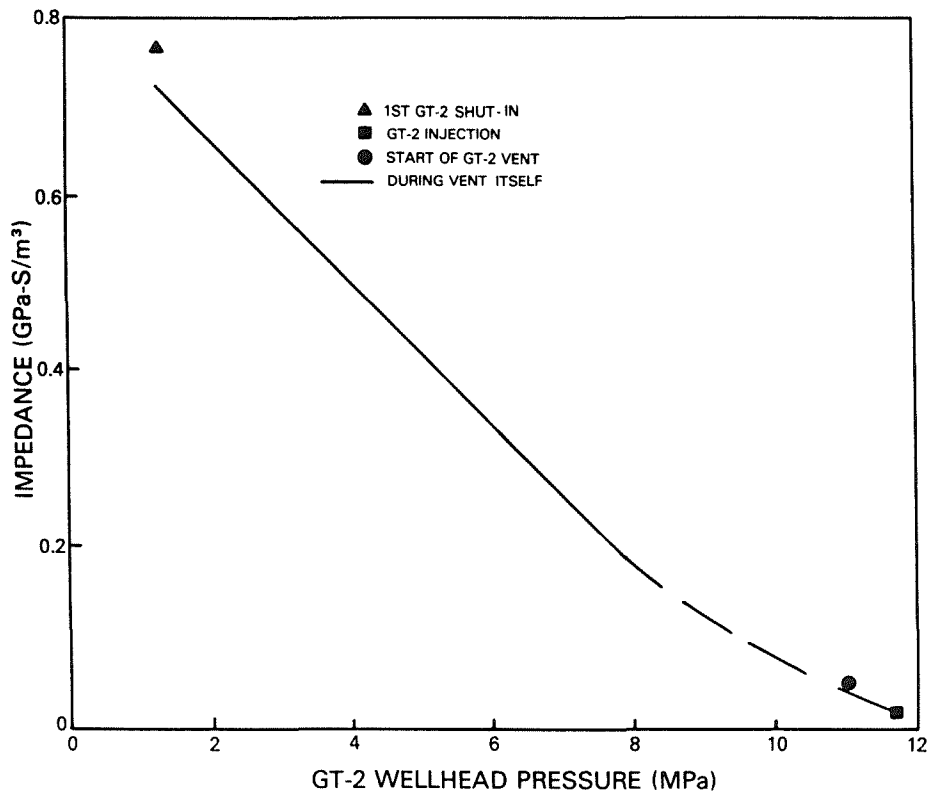

Fig. 9.
Approximate dependence of GT-2B outlet impedance upon GT-2B wellhead pressure.

average venting flow rate. The single huff-puff cycle of the experiment can be viewed in two ways. In mode I, it can be considered a complete early cycle of a high-pressure operation in which the EE-1 pressure is to oscillate about a pressure of 12 MPa (1700 psi), which is substantially greater than the usual operating pressure of 8 MPa (1200 psi) at which the water losses were satisfied during Run Segment 5. In mode II, it can be considered part of a low-pressure operation, of which only part of the vent cycle is present. The vent cycle was terminated to allow time for the subsequent impedance measurement, in which quasi-steady conditions were desired for a high-quality measurement. For mode I the EE-1 pressure would oscillate about an intermediate value of 8 MPa, for which the water losses have been completely satisfied. Even though the vent was terminated prematurely, the vent flow rate can be extrapolated to give approximate vent duration and flow rates. A linear extrapolation of the flow rate from the existing data (Fig. 8) will give lower limits to the vent duration, flow rate, and vent volume. The results of this extrapolation are included in Table I with the important parameters for both mode I and mode II operation.

It can be seen from this summary that both modes have reasonable cycle lengths and high average-vent-flow rates that are necessary for the operation of a huff-puff system. The estimated water losses are consistent with the pressurization state of the reservoir and can be expected to decline in the same manner as in the flow-through experiments.

III. MICROSEISMIC OBSERVATIONS

The SUE experiment has provided a new series of microseismic events that were released by increased pressurization of the EE-1/GT-2B fracture system. For the first time this type of activity was monitored by two widely separated downhole-triaxial-geophone stations [at 2697 m (8850 ft) in GT-2B, and 2918 m (9575 ft) in EE-2, true vertical depth]. Initial estimates indicate that over 15 000 events (detected and recorded at both stations) were caused by the 7 h of pressurization. None of these events were large enough to be detected by the surface seismic systems even though these experienced low background activity during the pressurization.

12

TABLE I

HUFF-PUFF CHARACTERISTICS

			Mode I High Pressure	Mode II Low Pressure
Pressures (MPa)	EE-1	Max Ave Min	15.2 11.7 8.3	15.2 6.9 3.5
	GT-2	Max Ave Min	12.4 6.9 1.5	12.4 low 1.5
EE-1 Injection		Flow rate (m³/s) Duration (h) Volume (m³)	4.1×10^{-2} 6 1000	4.1×10^{-2} 6 1000
GT-2B Vent		Flow rate (m³/s) Duration (h) Volume (m³)	1.3×10^{-2} 6 340	0.69×10^{-2} 36 >950
Water Loss		Fraction of injected volume	0.6	<0.1

In this section we discuss the following:

● Event rate history.

● Event rate vs EE-1 pressure.

● Map of larger events as recorded in GT-2B.

● S-P delay histories for selected events as recorded at each station.

● Signal-amplitude vs signal-duration study.

● Cumulative number of events vs signal-magnitude study.

The downhole monitoring systems were similar to those used in previous experiments (Refs. 4-7) as was most of the recording equipment. The events were recorded and monitored by the following equipment:

- Tape recorder.
- Two Hewlett-Packard 8-pen strip recorders that displayed the surface seismic net output, the output from six geophones, and the EE-1 pressure.
- Biomation scanning of horizontal geophone output from both stations, which produced plots of selected events in real time during the experiment.

The tape recordings and strip recorders had WWV channels for accurate time basing. The analogue tapes were used later to produce both digital tapes containing the larger events and continuous oscilloscope strip charts containing the filtered (100 Hz High Pass) output from selected geophone channels. The digital tapes were then used in the production of the event maps by techniques described in earlier reports (Refs. 4-6). The strip charts that contained the least noisy horizontal-geophone component from each station, along with the WWV time code, were examined for all events that appeared to be seismic in nature and that were recorded at each station. The peak-to-peak maximum amplitudes were measured for all signals on one channel for several half-hour periods along with the signal time duration (measured from signal onset to estimated time at which the signal disappeared into the background) for a number of events (spanning the range of observed amplitudes). The results are presented below.

A. Event Rate History and Event Rate vs Pressure

Estimates of the rate of events were obtained from the Hewlett-Packard strip chart at various times during the pressurization and subsequent shut-in. Figure 10, which is similar to Fig. 1 except for the superposition of microseismic event rate, shows an increasing event rate with time until the cessation of pumping into EE-1, at which time the rate drops sharply. Figure 11 plots these same event rates against the EE-1 pressure. Judging by the pressure at the commencement of activity and the pressure at the sharp increase in activity, this plot seems to indicate a threshold for seismic activity between 9.5 MPa (1400 psi) and 11.0 MPa (1600 psi), along with another apparent critical pressure of 15.0 MPa (2200 psi) at which seismic activity increases sharply. Examination of the EE-1 pressure history in either Fig. 1 or 10 shows a constant pressure level at this last pressure during the last 2 h of pumping, indicating the onset of further hydraulic fracturing. Additional fracturing was confirmed by the tracer experiments performed before and after

14

SUE. As explained later, the modal volume of the fracture system increased by about 40% as a consequence of SUE. Better measurements of the event rate using the oscillograph recordings should be useful in further examination of these relations.

B. Map of Events Recorded at the GT-2B Station

The initial map showing a plan view of 150 selected events recorded in GT-2B is shown in Fig. 12. The GT-2B geophone events were selected because this station contained dual inclinometers whose output allowed orientation of the geophone array. The locations of the seismic stations and the injection zone in EE-1 are also indicated. We located events during this experiment using a new location technique utilizing the S-P times and the relative delays measured in EE-2 along with the azimuths of the events recorded by the GT-2B geophones. Because we knew the azimuth measured from the GT-2B geophones and the distances from both geophone packages, GT-2B and EE-2, we could measure dips without actually using the output of the vertically oriented geophones. This follows because knowing the azimuth and radial distance with respect to GT-2B defines a unique circle in three-dimensional space. Knowing only the distance from EE-2 defines a sphere. Intersections of the circle and the sphere define only two possible points in space. We were able to eliminate one of these two possible locations by comparing the azimuth recorded at GT-2B with the relative polarization direction recorded by the EE-2 geophones. The complete geometrical location of the microseismic events without the vertically oriented geophones was fortunate because the vertical geophones may not have been working properly due to large inclinations of both wells from the vertical.

Figure 13 shows event locations from three previous experiments, Expts. 203, 195, and Run Segment 4, projected in plan view. Fracturing experiments 203 and 195 were conducted on March 14, 1979 and March 21, 1979, respectively. The microseismic events during the 1-day experiments, 203 and 195, are confined to a fairly narrow zone that trends in the north-northwest direction, but the events measured several days after the beginning of Run Segment 4 indicate considerable lateral departure from this narrow zone, caused by additional diffusion of the injected water. Figure 14 shows the plan views of the SUE microseismic events sequenced in time, in nearly 1-h increments. In examining these sequences it should be recalled from Fig. 10 that pressurization began about 16:00. As can be seen, the north-by-northwest-trending seismic
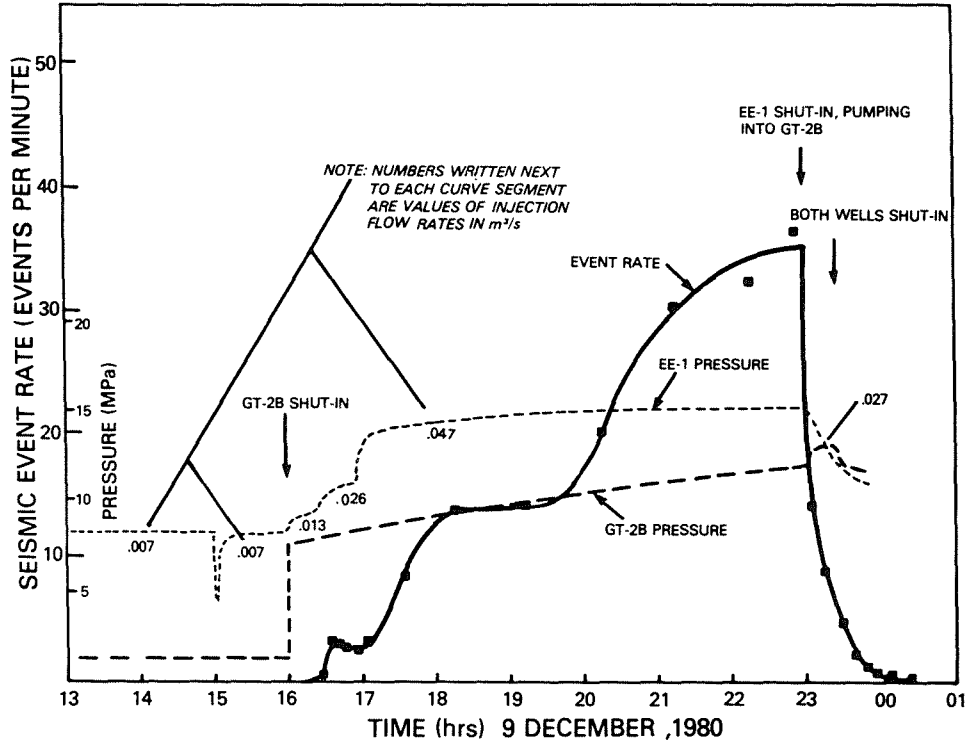
Fig. 10.
System pressures, pumping rates, and seismic event rates during SUE.
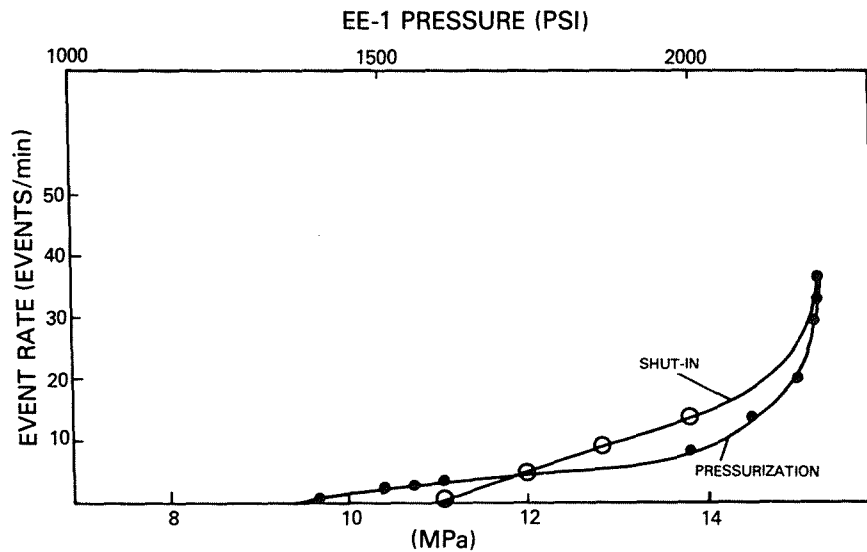

Fig. 11.
Seismic event rate as function of EE-1 wellhead pressure.

zone, so prominant during experiments 203 and 195, is still apparent in the SUE data, but there is some tendency for the microseismic events to spread laterally--in the last sequence, from 22:09 to 23:10, this spreading amounts to about 200 m. Figure 15 shows the events projected on a vertical north-south-trending plane. Most of the events are concentrated within a circular zone with an area of 60 000 m^2. As discussed in the report on Run Segment 5 (Ref. 1), the seismic area so determined in SUE is in qualitative agreement with heat-transfer areas determined by modeling the thermal drawdown of the reservoir.

C. S-P Delay Histories For Selected Events

Further reduction of the data on the analogue tapes is still being pro-cessed to provide measurements of the P- and S-wave delay as measured at each station. These measurements, along with measurements of the S-P delay at the EE-2 station, should remove most of the ambiguities arising from centro-symmetry as described in Ref. 6. However, a series of playbacks were obtained from the Biomation digital oscilloscope during the pressurization. An example is shown in Fig. 16 in which the two horizontal channels for each station are displayed. An approximate S-P delay was easily obtained for most of these randomly selected events, and Figs. 17 and 18 show the changes in these delays with time in GT-2B and EE-2, respectively. The envelope for each group pro-vides a rough measure of the movement of the events relative to both stations.

D. Signal Amplitude vs Signal Duration Study

In statistical studies of sequence of seismic events the usual parameter against which the frequency or cumulative number of events is plotted is the local magnitude, M_L. The local magnitude scale is defined, Ref. 8:

$$M_L = 2.79 \log T - 3.63 \quad ,$$

where T is the signal duration in seconds. The signal duration is, however, difficult and tedious to measure and therefore a relation between the duration and maximum peak-to-peak amplitude as measured on the strip chart has been developed. This relation is based upon the SUE data, using initially deter-mined values of T. Figure 19 shows a plot of these data accompanied by the best power curve fit to the data. This curve has the equation
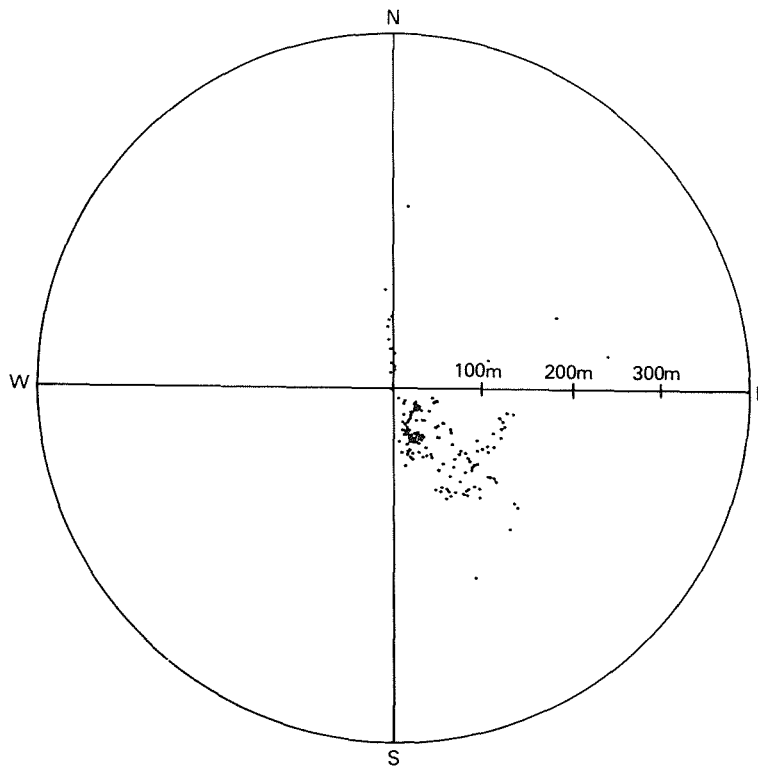
Fig. 12.
Map (plan view) of seismic events recorded at the GT-2B station.
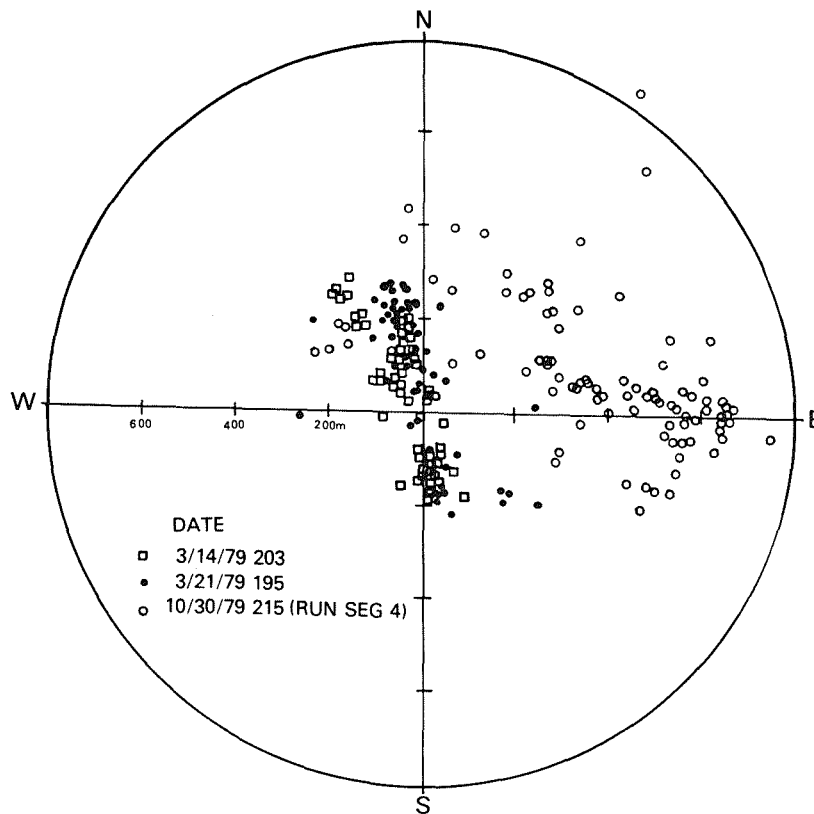

Fig. 13.
Map (plan view) of seismic events located during previous Expts. 195, 203, and 215.
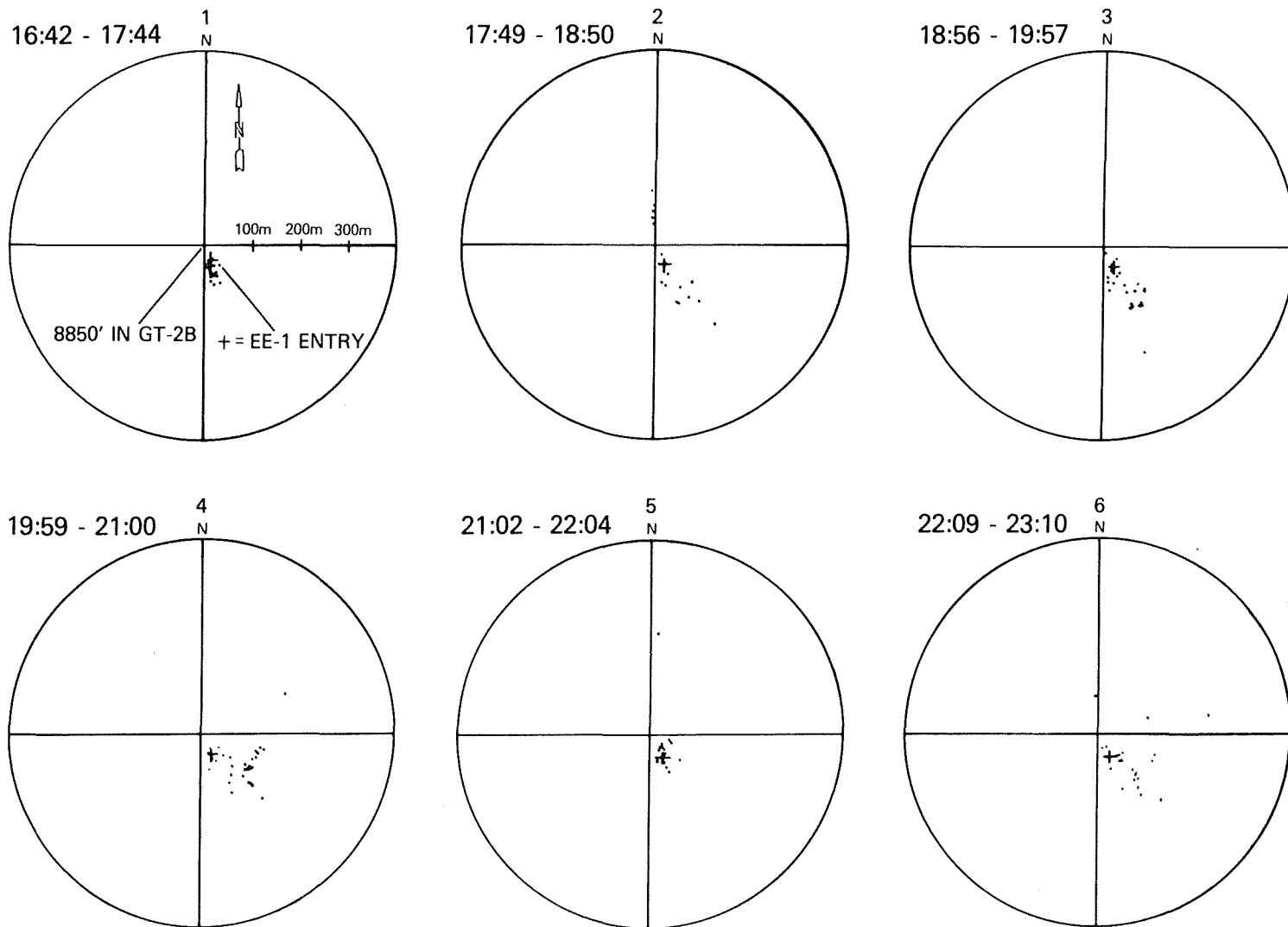
18

16:42 - 17:44

17:49 - 18:50

18:56 - 19:57

19:59 - 21:00

21:02 - 22:04

22:09 - 23:10

100m 200m 300m

8850' IN GT-2B

+ = EE-1 ENTRY

Fig. 14.

Maps (plan views) of seismic events located in six equal-time intervals during the EE-1 and GT-2B injections of the SUE experiment.
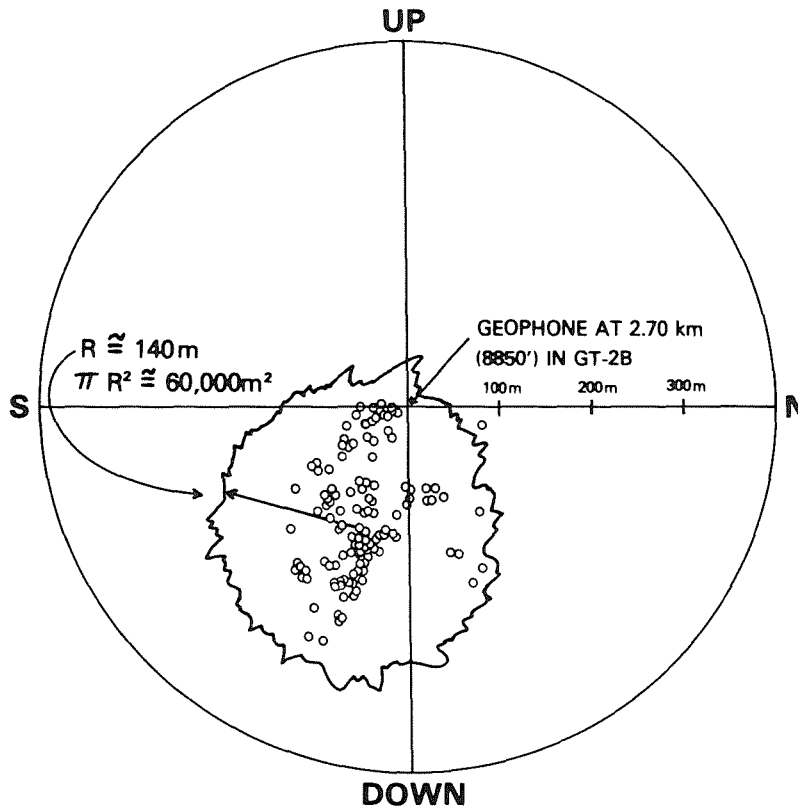
Fig. 15.
Elevation view of SUE events recorded at GT-2B. Events are projected on a verti-
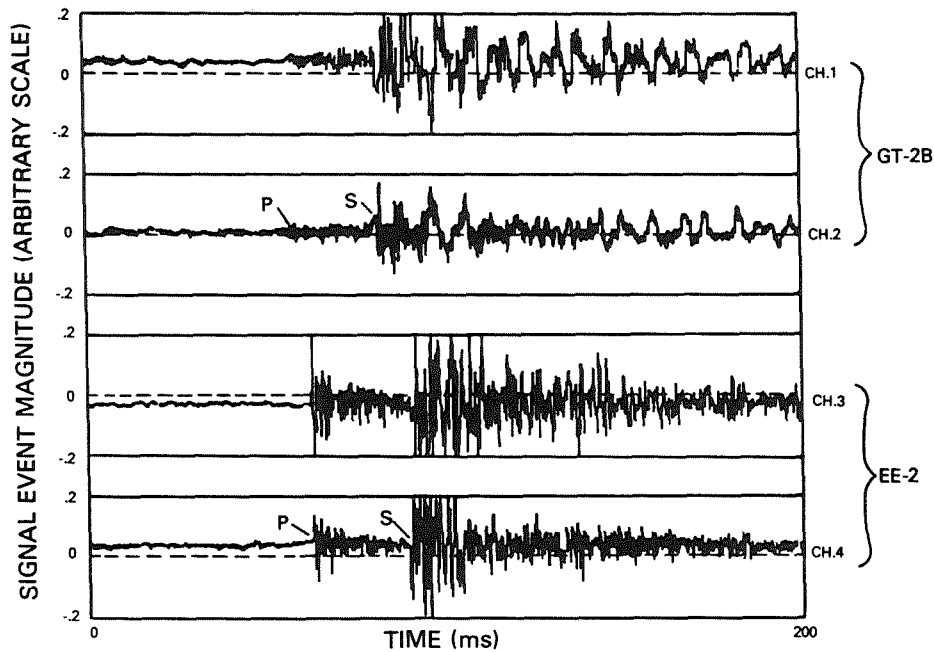cal, north-south-trending plane.

Fig. 16.
Biomation digital oscilloscope playback showing the characteristics of a typical
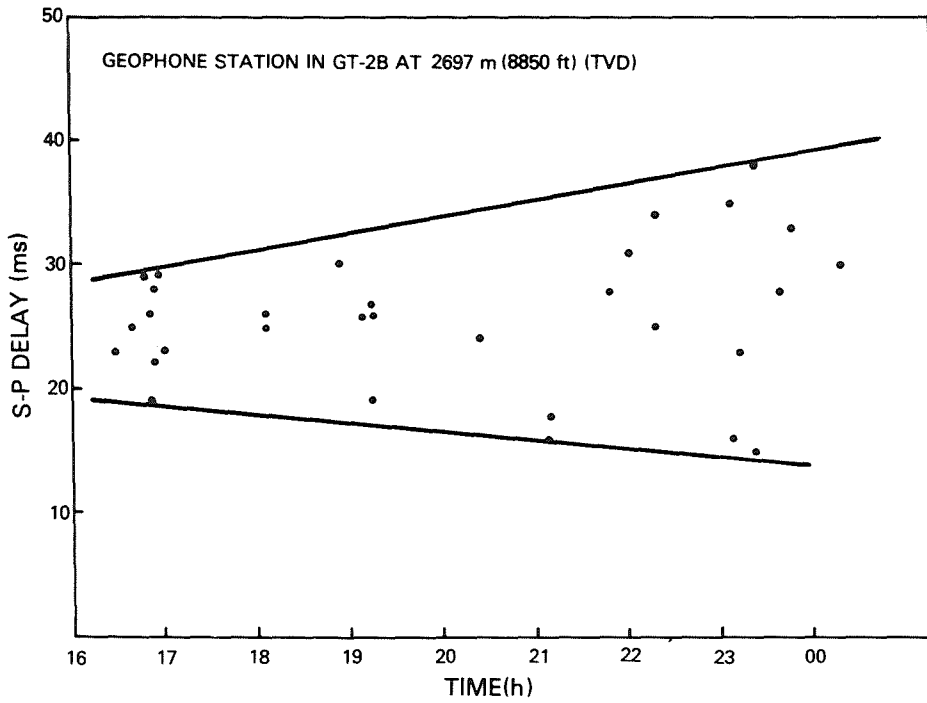microseismic event as received on the horizontal geophone.

20

GEOPHONE STATION IN GT-2B AT 2697 m (8850 ft) (TVD)

Fig. 17.
Envelope of S-P delay times for events received at GT-2B vs time.
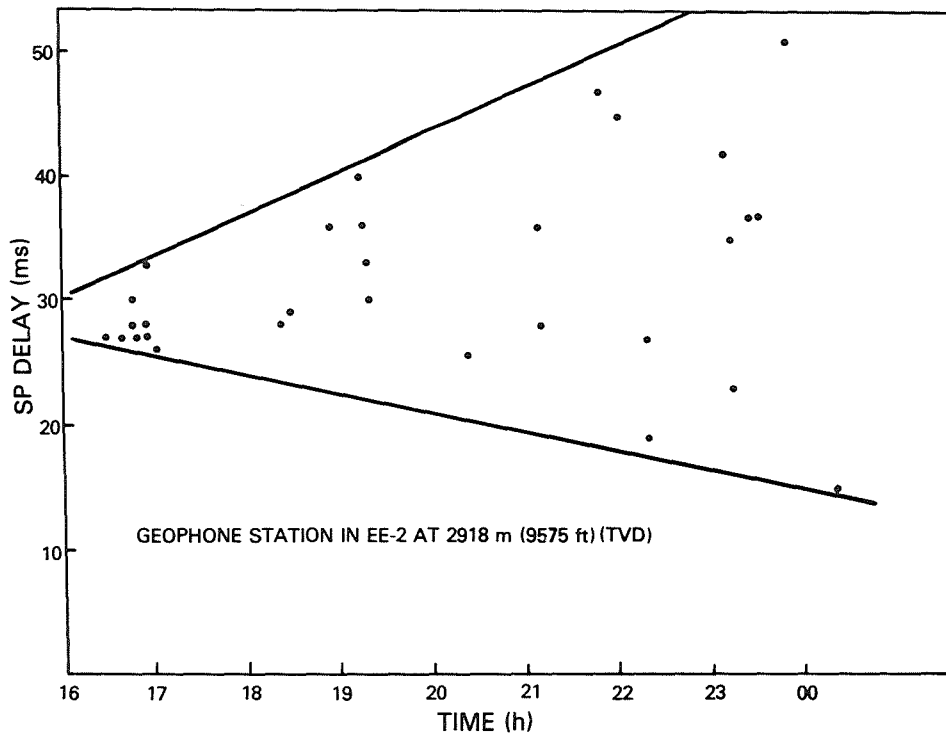

GEOPHONE STATION IN EE-2 AT 2918 m (9575 ft) (TVD)

Fig. 18.
Envelope of S-P delay times for events received at EE-2 vs time.

$$A = 65.6T^{1.82} \quad , \tag{4}$$

where A is the peak-to-peak chart am-
plitude in mm.

Combining the two equations gives
the local magnitude as a function of
the measured amplitude:

$$M_L = 1.54 \log A - 6.42 \quad . \tag{5}$$

This equation is used below in deter-
mining the amplitude range for a given
magnitude interval.

E.   Cumulative Number vs Signal
    Magnitude Study

Figure 20 shows a portion of the
oscillograph record on which numerous
seismic signals of varying amplitude
are present. To avoid spurious signals
due to geophone package movement in the

Fig. 19.
Plot of event amplitudes vs event dura-
tions along with best-fit power curve.

wells, the amplitudes were measured only for those signals present on the EE-2

Fig. 20.
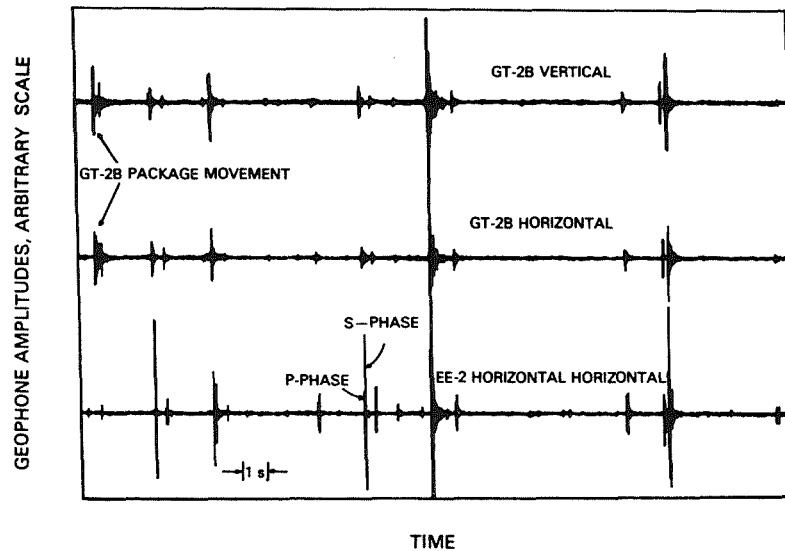Typical portion of oscillograph output of filtered analogue tape data recorded
from components in GT-2B and EE-2.

22

horizontal-geophone channel that had nearly simultaneous signatures on the GT-2B horizontal channel. The number of signals with amplitudes bounded by values computed from Eq. (5) for magnitude intervals of 0.25 were tabulated over the magnitude range -6.25 to -3 and for a given time interval (typically 0.5 h). Figure 21 shows the log of the cumulative sum (number of events with magnitudes greater than a given magnitude) vs magnitude for three time intervals during the EE-1 injections. Typically normal seismic sequences show similar linear plots with slopes (the so-called b-values) ranging from -0.5 to -1.5; our b-values range from only -0.62 to -0.65. Of interest is the major change in the relative number of large events as indicated by the departures in each of the lines in Fig. 21 that start at a magnitude of about -3.5. Of even greater interest is the energy of these larger events (say those with M_L > -3). Using the energy-magnitude relation defined by Richter (9) the relative energies for each time interval were computed and are shown in Table II.

Even though the reservoir was continually being stressed to higher levels, the production of the larger events took a dramatic drop along with released energy during the later stages of pumping. This suggests that these events were associated with the thermally drawn-down region of the reservoir and that most of this stored strain had been released by the initial pressurization.

IV. PRESSURE OSCILLATIONS

Analytical models (Refs. 10 and 11) and experimental results (Ref. 12) suggest that both free and forced oscillations of the pressure in a HDR system can yield information about fracture size or impedance. During the EE-1 and GT-2B high-pressure injection-phases, valve operations and piston pump strokes

TABLE II

RELATIVE ENERGIES

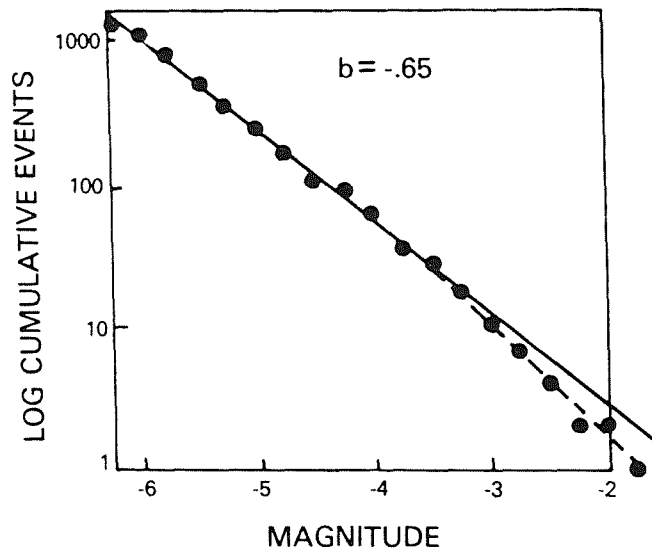| Time Interval	Pressure (MPa)		Number of Events with Magnitude > -3	Relative Energy
	EE-1	GT-2B		
17:00-17:30	13.3	5.6	4	1
19:00-19:30	14.8	10.1	10	19
22:09-22:39	15.2	11.6	2	5

(a) TIME DURATION
17:00-17:30
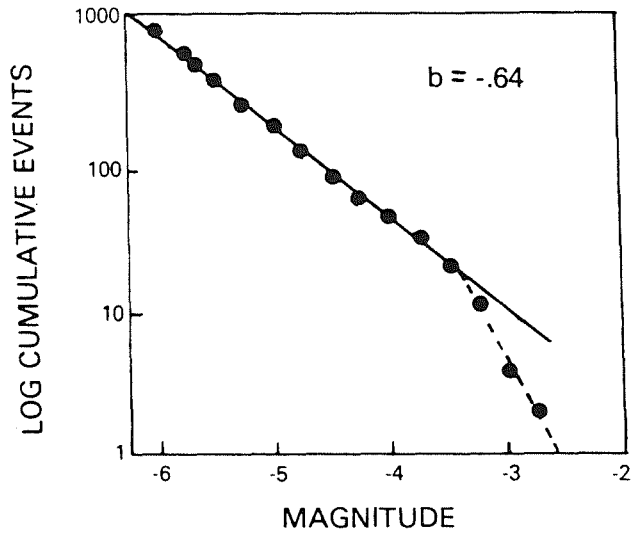
(b) TIME DURATION
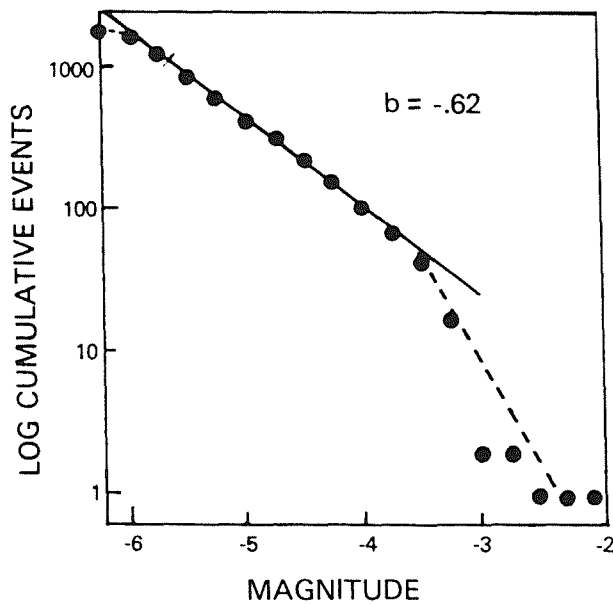19:00-19:30

(c) TIME DURATION
22:09-22:39

Fig. 21.
Cumulative frequency vs local
magnitude plots for EE-2
station data.

could stimulate such oscillations. Therefore arrangements were made to record and monitor possible oscillations. Both the wellhead pressures of GT-2B and EE-1 and the amplified oscillations of the wellhead pressures about their mean values were recorded by chart-recorder and on magnetic tape (Ampex FR 3020).

Oscillations of the wellhead pressures were observed in two different frequency ranges:

(1) Between 2 and 30 Hz the Halliburton pumps produced very narrow-banded noise with pressure amplitudes of about 1 bar at the wellhead of EE-1. Changes in the pertinent line spectra are mainly due to changed flow rates. It is hard to tell if the remaining differences within the same flow-rate interval are caused by changes in reservoir spectral response (which might be due to altered fracture size or inlet impedance) or by varying pump operation (Fig. 22). In this frequency range no signal above noise level was trans-mitted through the reservoir to the GT-2B wellhead.

(2) Shut-ins, decreases of flow-rate, venting, and other valve opera-tions triggered damped harmonic oscil-lations in the frequency range between 0.1 and 0.3 Hz. They are believed to be longitudinal (compressional) oscil-lations of the water in the wellbore. Their natural frequencies appear to be those of a fundamental mode oscilla-tion, implying that the inlet depth corresponds to a quarter of a wave length. The wellhead was shut in for all the observed cases, so the water was displaced from the borehole into the reservoir and back again.

The damping of these oscillations may be due to the viscosity of the water column, but could also contain information about changes of inlet impedance. However, there is no sig-nificant change in the damping con-stants of the observed oscillations
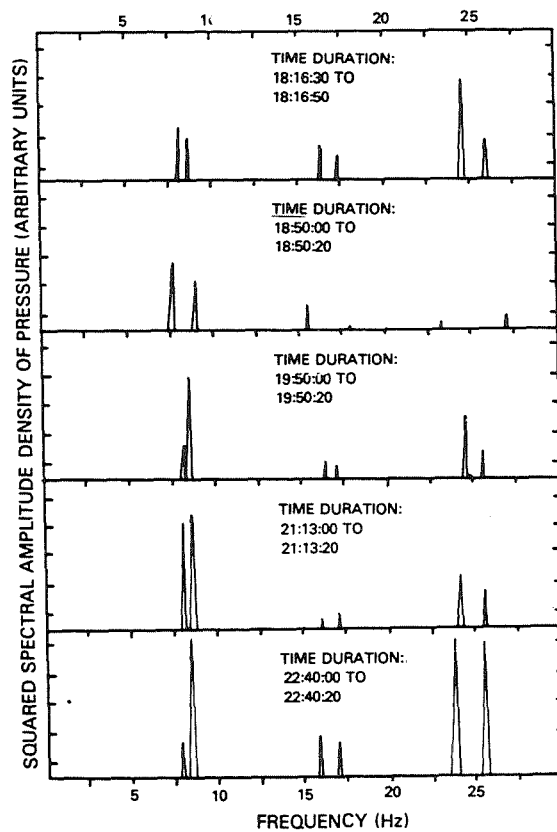

Fig. 22.
Spectral analysis of pressure oscilla-tions during EE-1 injections.

(Fig. 23). These oscillations were mainly stimulated in the wellbore where the valve operations were performed, but with two exceptions: the switching from Los Alamos pumps to Halliburton pumps at the EE-1 wellhead caused an oscillation in GT-2B, and the beginning of the vent of GT-2B triggered one in EE-1.

(3) During the venting of GT-2B, a long-period oscillation with a period of 454 ± 2 s was observed for 3 h. The pressure deviations were nonharmonic but the frequency was constant, that is, independent of pressure. At first it was thought that this constant-frequency response might be due to elastic opening and closing of the fracture system, but eventually it was attributed to a pressure-activated control valve. The failure of two pressure regulators in the supply line to the control valve, FCV-2, resulted in the control valve's fluctuating, with the normal pressure fluctuations produced by the air compressor.

V. POST-SUE IMPEDANCE MEASUREMENT

As mentioned in the introduction, following the vent from the high-pressure levels during SUE, normal Run Segment 5 loop operations were resumed at 06:20 on December 10, and continued until 09:00 on December 16. This period of loop operation provided an opportunity for measuring the post-SUE reservoir impedance. This measurement differs from the impedance estimates in Sec. II in that quasi-steady conditions prevailed for several days. The quasi-steady measurement is the one we usually measure, and a post-SUE measurement under these quasi-steady conditions was desired for comparison to the one obtained before SUE.

Figure 24 shows the overall reservoir impedance history just before and just after SUE. The total impedance involves a buoyancy correction that was calculated to be 2 MPa (300 psi). The entrance and exit impedances are derived from shut-in experiments on the dates shown. The techniques for determining entrance and exit impedances are based upon Muskat analysis of the wellhead pressures during shut-ins of EE-1 and GT-2B, respectively. Background discussion of this type of analysis is found in Ref. 7, and the complete
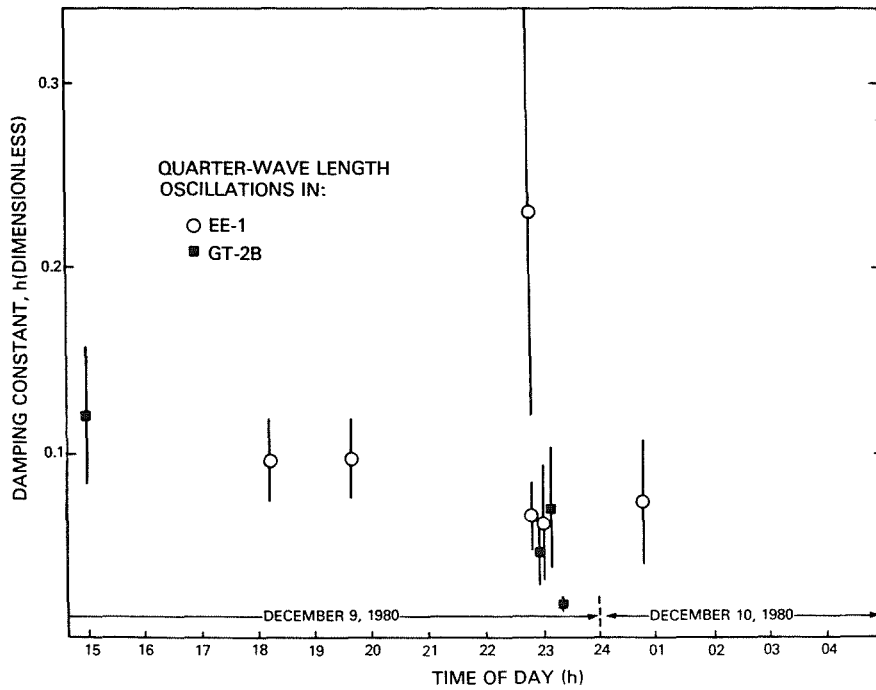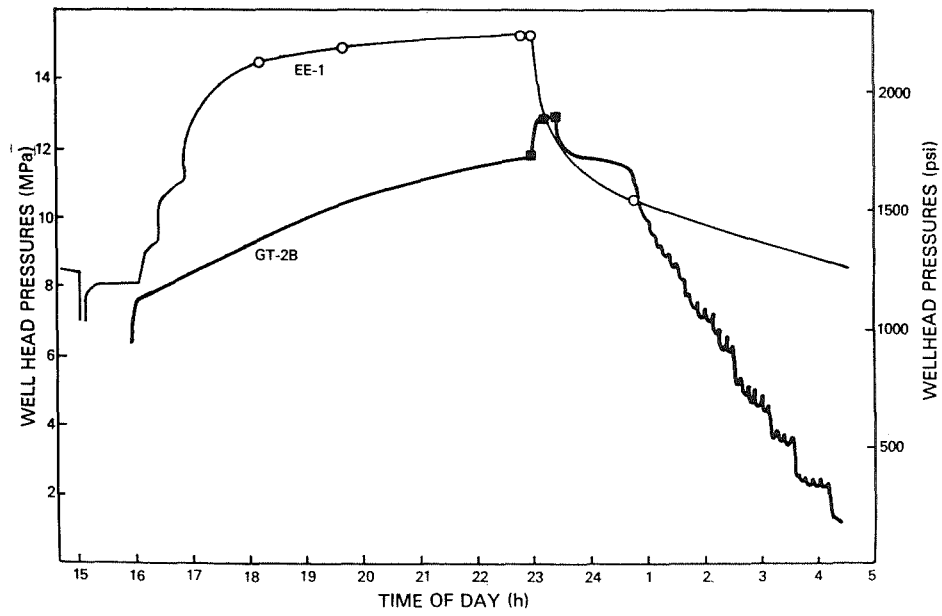
26

Fig. 23.
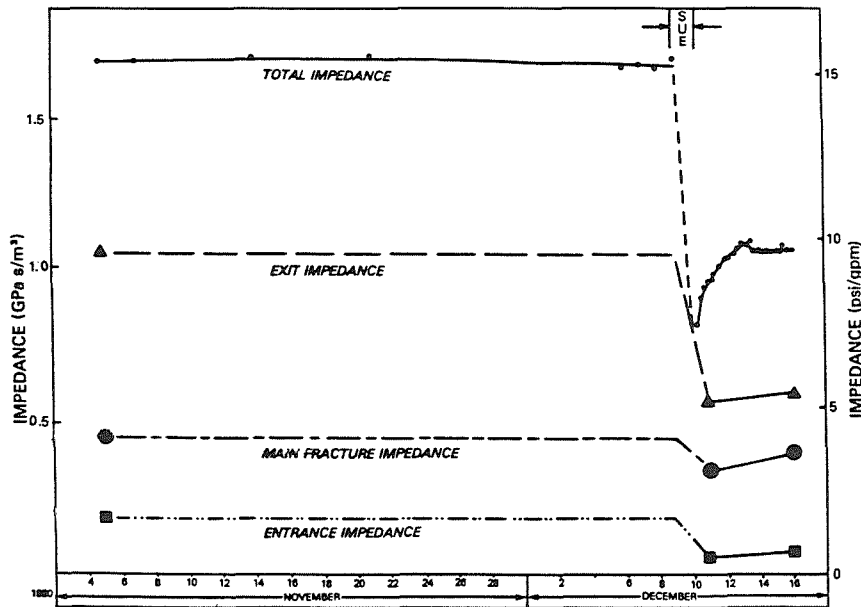Damping constants of oscillations in the boreholes.

Fig. 24.
Effect of Stress Unlocking Experiment (SUE) on impedances.

details of all the Run Segment 5 shut-ins, before and after SUE, are presented in an internal technical report.*

The results of the experiment are summarized in Table III, which shows the percentage decrease in the impedance values.

TABLE III

CHANGES IN IMPEDANCES CAUSED BY SUE

Type of Impedance	(a) Before, GPa s/m³ (psi/gpm)		(b) After, GPa s/m³ (psi/gpm)		Percent Decrease (a-b)/a x 100
Total	1.42	(15.5)	0.90	(9.8)	37
Entrance	0.16	(1.7)	0.06	(0.7)	61
Exit	0.90	(9.7)	0.50	(5.5)	43
Main Fracture	0.38	(4.1)	0.34	(3.7)	12

*R. L. Aamodt, "Distributed Impedances in the EE-1/GT-2B Circulation System During Run Segment 5 (Phase 1, Experiment 217) As Determined From Shut-in Experiments," Los Alamos National Laboratory internal report Tech Memo #1, January 23, 1981.

VI. TRACER STUDIES

In order to characterize the changes in fracture-system volume and flow distribution produced by the SUE experiment, radioactive NH_3Br^{82} tracer experiments were conducted before and after the SUE. In both cases, a 400-mCi pulse of tracer was injected and was monitored by logging with a downhole gamma counter in addition to counting at the production wellhead with a NaI crystal detector. The pre-SUE tracer test was run on December 2, 1980, and the post-SUE tracer test occurred on December 12, 1980.

Flow conditions and preliminary results of these tests are compared in Table IV with other tracer experiments, using Na-Fluorescein dye, as well as radioactive Br tracers during Run Segments 4 and 5. In this table, only the modal volume is presented for comparison. Previous presentations of the tracer results (Ref. 7) have also compared the integral mean volume. However, as is shown in the last column of Table IV, for several tracer experiments the sampling was terminated before background was reached, and the integral mean volumes include varying amounts of the long residence-time data. Because of equipment malfunction, the data for the pre- and post-SUE experiments were recorded by hand at roughly 1-h intervals. Unfortunately, data for the 6-h period centered at about the modal volume in the pre-SUE experiment was not recorded. The modal value presented in Table IV was found by superimposing the data measured downhole with the data measured at the surface. The mode of the downhole data was then adjusted for the transit time to the surface to give the mode in the surface data.

Comparison of the modal volumes from the Segments 4 and 5 experiments show a regular increase of the modal value with time. This increase in volume is attributed to thermal contraction effects due to heat extraction and is analyzed in more detail below. A rather large change in the modal volume is observed in Fig. 25 after the pressurization of the system during SUE. The high injection pressure of 15 MPa (2200 psi) was sufficient to increase the modal volume from 187 to 266 m^3, a 43% increase in size. Comparison of the normalized residence time distributions for the last 3 tracer experiments (not presented here) shows no corresponding change in dispersion characteristics due to the SUE experiment. Apparently the volumes of the existing fractures were increased with no new fractures or other changes in flow paths being created. Detailed studies of these effects will be considered in a subsequent report.

TABLE IV

SUMMARY OF DYE AND RADIOACTIVE TRACER EXPERIMENTS

Experiment and Date	Tracer[a]	EE-1 Injection Pressure MPa	GT-2B Production Pressure MPa	GT-2B Production Flow Rate (m³/s)	Average[b] Production Temperature (°C)	Cumulative Power Extracted During each Run Segment (10⁶KW-h)	Modal[c] Volume (m³)	Integral Mean Volume (m³)	Total Produced Vol During Tracer Test (m³)
Run Segment 4									
10/26/79	F	17.2	1.1	0.0064	153.	0.1	136.	207	469
10/29/79	F	17.2	10.3	0.0081	154.	0.3	144.	230	619
11/2/79	F	9.3	1.1	0.0066	153.	0.6	121.	262	570
11/12/79	F	9.3	1.1	0.0064	153.	1.3	129.	283	662
Run Segment 5									
4/15/80	F	9.8	1.3	0.0075	158.	1.6	155.	404	1440
5/9/80	B	9.5	1.3	0.0071	158.	2.8	161.	1100	3030
9/3/80	B	8.8	1.3	0.0070	154.	7.5	178.	1511	4140
12/2/80 (Pre-SUE)	B	8.5	1.1	0.0065	149.	11.1	187.	581	1310
12/12/80 (Post-SUE)	B	8.4	1.3	0.0098	149.	11.4	266.	1118	2690

[a]F = Sodium fluorescein dye, B = ^{82}Br.

[b]Reservoir outlet temperature measured downhole.

[c]Modal Volume is defined as the volume of tracer circulated through the fracture system from time of entry until that time at which the tracer concentration at the outlet is maximum. We believe this volume. to be the most easily measured one, as well as the most unambiguous one for making comparisons of the effect of pressure or temperature or fracture size.
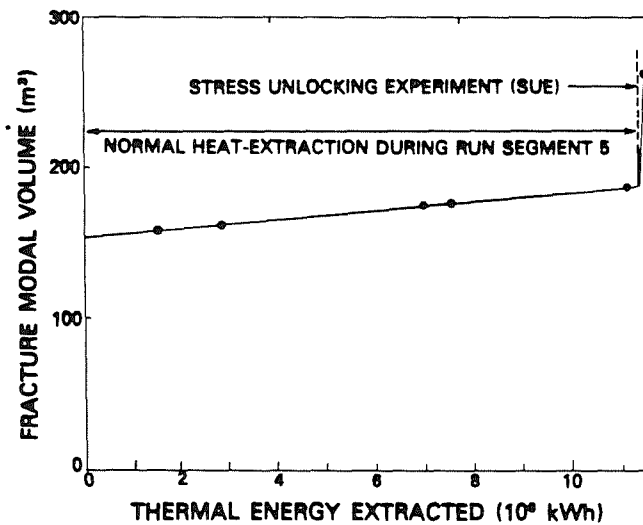

Fig. 25.
Fracture modal volume increases due to Run Segment 5 heat extraction and high-pressure injection during SUE. The thermal energy referred to here is limited to that of the reservoir only--it excludes the contribution from the injection and production wellbores. Thus the total energy during Run Segment 5 was 15 x 10⁶ kWh.

Figure 25 indicates a reasonably linear increase of fracture modal volume as heat was extracted; a total heat extraction, E, resulted in a volume increase, ΔV, of 37 m^3. The energy E is related to the integral of the temperature decrease over the entire reservoir rock volume affected by thermal drawdown. If the rock is assumed to be a stress-free, freely contracting media, then ΔV is also related to the same integral, and it can be shown that

$$\Delta V = \alpha_v E / (\rho c)_r \quad ,$$

where α_v is the volumetric thermal expansion coefficient of the rock and $(\rho c)_r$ is its volumetric heat capacity. Using a typical value, $(\rho c)_r = 2.7 \times 10^{-6}$ J/(m^3 °C), and the preceding values of ΔV and E, α_v can be estimated as 2.8 $\times$ 10^{-6}/°C. This is only one-tenth the value typical of laboratory experiments with dense granite (Ref. 13). The large discrepancy is attributed to two causes: (1) the rock is actually under considerable tectonic stress, and much of the expected thermal contraction simply was consumed in relieving a part of these stresses; and (2) much of the thermal contraction may have been manifested as an increase in porosity that occurred far enough away from the main fracture system that the porosity increase was not detected by the tracer passing through the fracture system. It is interesting to note that SUE itself resulted in another ΔV of 78 m^3, so that the total volume increase was 115 m^3, still only 30% of that expected if the reservoir was completely free to contract.

VII. CONCLUSIONS

- The high-pressure phases of SUE resulted in a reduction of overall reservoir impedance by 37%, from 1.42 GPa s/m^3 (15.5 psi/gpm) before SUE to 0.9 GPa s/m^3 (9.8 psi/gpm) after SUE. Most of the reduction took place at the reservoir exit where the impedance was reduced from 0.90 to 0.50 GPa s/m^3 (9.7 to 5.5 psi/gpm).

- High pressure also caused a 43% increase in fracture-system modal volume, from 187 to 266 m^3.

- The substantial reduction in impedance and increase in fracture size has further improved the chance for success in using the Huff-Puff mode of heat extraction. The SUE experiment also indicates that the present system can be operated in the Huff-Puff mode with good flow

characteristics. That is, the system now has reasonable water losses, high vent volume, and a high venting flow rate.

- The use of two separated geophone stations has significantly increased knowledge of absolute event location and may allow estimation of rock properties such as local acoustic velocity and attenuation. The geophone packages performed superbly throughout SUE.

- The high degree of linearity of the event frequency/magnitude relations measured during this experiment (Fig. 21) strongly suggests that a single seismic mechanism, most likely shear failure, was the cause for the entire event sequence (magnitude range from -7 to -1.5).

- The peak in the rate of larger events near the middle of the pumping sequence with an accompanying maximum of energy release is indicative of the release of stored stress, most likely arising from the prolonged thermal drawdown of the reservoirs.

REFERENCES

1. G. A. Zyvoloski (Ed.), "Evaluation of the Second Hot Dry Rock Geothermal Energy Reservoir: Results of Phase I, Run Segment 5," Los Alamos National Laboratory report LA-8940-HDR (to be published).

2. H. N. Fisher and J. W. Tester, "The Pressure Transient Testing of a Man-Made Fractured Geothermal Reservoir: An Examination of Fracture Versus Matrix Dominated Flow Effect," Los Alamos Scientific Laboratory report LA-8535-MS (September 1980).

3 D. W. Brown, (Ed.), "Results of Experiment 186, The High Back-Pressure Flow Experiment," Los Alamos National Laboratory report LA-8941-HDR (to be published).

4. A. G. Blair, J. W. Tester, and J. J. Mortensen, "LASL Hot Dry Rock Geothermal Project: July 1, 1975-June 30, 1976," Los Alamos Scientific Laboratory report LA-6525-PR (October 1976).

5. Laboratory HDR Project Staff, "HDR Geothermal Energy Development Project Annual Report Fiscal Year 1974," Los Alamos Scientific Laboratory report LA-7109-PR (February 1978).

6. M. C. Brown, R. B. Duffield, C. L. B. Siciliano, and M. C. Smith, "HDR Geothermal Energy Project: Annual Report Fiscal Year 1978," Los Alamos Scientific Laboratory report LA-7807-HDR (April 1979).

7. H. D. Murphy, (Ed.), "Preliminary Evaluation of the Second Hot Dry Rock Geothermal Energy Reservoir: Results of Phase 1, Run Segment 4," Los Alamos Scientific Laboratory report LA-8354-MS (May 1980).

8. G. M. Cremer, R. B. Duffield, M. C. Smith, and M. G. Wilson, "HDR Geothermal Energy Development Project: Annual Report Fiscal Year 1979," Los Alamos Scientific Laboratory report LA-8280-HDR (August 1980).

9. C. F. Richter, Elementary Seismology, (W. H. Freeman, San Francisco, 1958) p. 366.

10. G. Bodvarsson, "Dynamics of Liquids in Subsurface Spaces; Hydroelastic Oscillations and Waves," Report EAR77-23938 for the National Science Foundation, Parts (I) to (IV), Oregon State University, Corvallis, Oregon (1980).

11. G. Fras, "Reconnaisance de Certains Meilieux Rocheux et Théories des Systèmes," Thesis, Institute Nationale Polytechnique de Poulouse, France, 1979.

12. H. Keppler, "Versuche zur Anregung von Schwingungen in einem hydraulisch erzeugten Rißsystem," Bericht der Bundesanstalt fur Geowissenschaften und Rohstoffe, Hannover, Archiv Nr. 86882 (1980).

13. B. J. Skinner, "Thermal Expansion," in Handbook of Physical Constants, S. P. Clark, Jr., Ed., (Geological Society of America, New York, 1966).